Structural Engineering and Mechanics, *Vol. 63, No. 3 (2017) 361-370*
DOI: https://doi.org/10.12989/sem.2017.63.3.361

Experimental and numerical disbond localization analyses of a notched plate repaired with a CFRP patch

Sahli Abderahmane*[1], Bouziane M. Mokhtar[1], Benbarek Smail[1], Steven F. Wayne[2], Liang Zhang[2], Bachir Bouiadjra Belabbes[1] and Serier Boualem[1]

[1]*Laboratoire Mécanique Physique des Matériaux (LMPM), Department of Mechanical Engineering, University of Sidi Bel Abbes, Sidi Bel Abbes 22000, Algeria*
[2]*Medical Acoustic Laboratory, University of Memphis, Memphis, TN, USA*

(Received September 14, 2016, Revised April 22, 2017, Accepted April 25, 2017)

Abstract. Through the use of finite element analysis and acoustic emission techniques we have evaluated the interfacial failure of a carbon fiber reinforced polymer (CFRP) repair patch on a notched aluminum substrate. The repair of cracks is a very common and widely used practice in the aeronautics field to extend the life of cracked sheet metal panels. The process consists of adhesively bonding a patch that encompasses the notched site to provide additional strength, thereby increasing life and avoiding costly replacements. The mechanical strength of the bonded joint relies mainly on the bonding of the adhesive to the plate and patch stiffness. Stress concentrations at crack tips promote disbonding of the composite patch from the substrate, consequently reducing the bonded area, which makes this a critical aspect of repair effectiveness. In this paper we examine patch disbonding by calculating the influence of notch tip stress on disbond area and verify computational results with acoustic emission (AE) measurements obtained from specimens subjected to uniaxial tension. The FE results showed that disbonding first occurs between the patch and the substrate close to free edge of the patch followed by failure around the tip of the notch, both highest stress regions. Experimental results revealed that cement adhesion at the aluminum interface was the limiting factor in patch performance. The patch did not appear to strengthen the aluminum substrate when measured by stress-strain due to early stage disbonding. Analysis of the AE signals provided insight to the disbond locations and progression at the metal-adhesive interface. Crack growth from the notch in the aluminum was not observed until the stress reached a critical level, an instant before final fracture, which was unaffected by the patch due to early stage disbonding. The FE model was further utilized to study the effects of patch fiber orientation and increased adhesive strength. The model revealed that the effectiveness of patch repairs is strongly dependent upon the combined interactions of adhesive bond strength and fiber orientation.

Keywords: bonded/unbonded prestressing; composites; crack/damage detection/identification; finite element method (FEM); simulation

1. Introduction

Patch repair of metallic structures in modern aerospace applications employs advanced composite and adhesive technologies. Bonded composite repairs have proven to be cost-effective methods of repairing damaged aircraft wings and related sheet metal structures Baker (1993, 1995, 1997), Elhannani *et al*. (2016). The bonded repairs can be done in the field and offer many advantages; increased stiffness, reduced stress amplification around cracks or defects in the sheet metal with minimal additional weight. There are, however, limitations to this technique due to varying interfacial bond strength and relative stiffness to mating substrates. Baker *et al*. (2003), reported that patch repaired plates disbond, especially when repairs involve cracks and sharp notches. They also found that disbonding can affect the accuracy of tests, although disbonding was not quantified in their study. For Baker's work, one should use a safety factor when calculating the stress intensity factor of the repaired sample to take into account the effect of disbonding. Ouinas *et al*. (2012) conducted a disbond study on the composite patch repair of an aluminum plate with an imperfection of the initial bond between the patch and the plate: they found that the disbond increased the crack propagation rate. Bouiadjra *et al*. (2008, 2016), Aicha Benchiha *et al*. (2015, 2016) carried out a finite element analysis on the behavior of a crack repaired with a Boron/Epoxy patch by computing the stress intensity factor (SIF) of the crack tip in mode I and mixed mode. They also analyzed the disbond effect on the SIF behavior. They found that the disbond around the crack tip reduced the life of the cracked plate. Shin-etsu *et al*. (2007), Berrahou *et al*. (2016), conducted a numerical analysis to identify the location and shape of disbonding close to the crack front on CFRP repaired aluminum plate. They used an in-plane strain range ahead of the crack front as the criteria for disbonding and found that the disbond occurs all along the crack front. Denney *et al*. (1997) also studied patch repaired cracked plates considering full and partially bonded reinforcement configurations of various disbond locations and sizes. Their comparisons showed that there is a definite variation in fatigue life depending on the location and size

*Corresponding author, Ph.D.
E-mail: sahliabderahmen@yahoo.fr

ISSN: 1225-4568 (Print), 1598-6217 (Online)

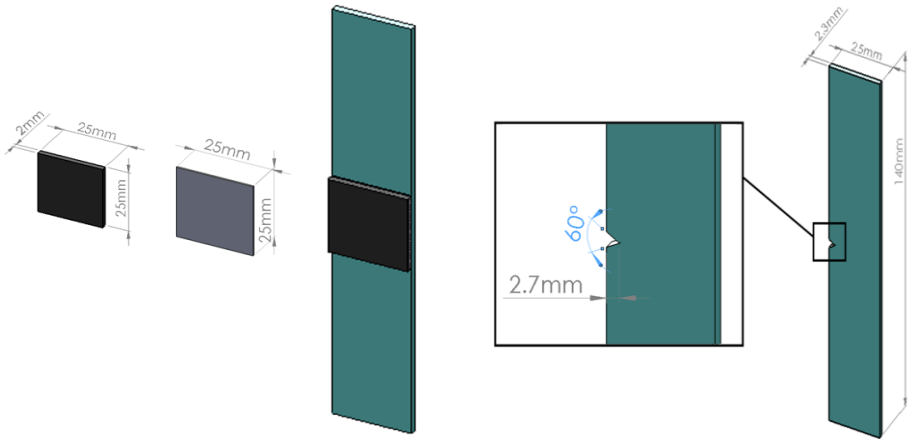

Fig. 1 Geometry of the tested sample, from left to right; the CFRP patch, the adhesive layer, the patch and adhesive assembly affixed to aluminum substrate and close-up of prenotched aluminum substrate

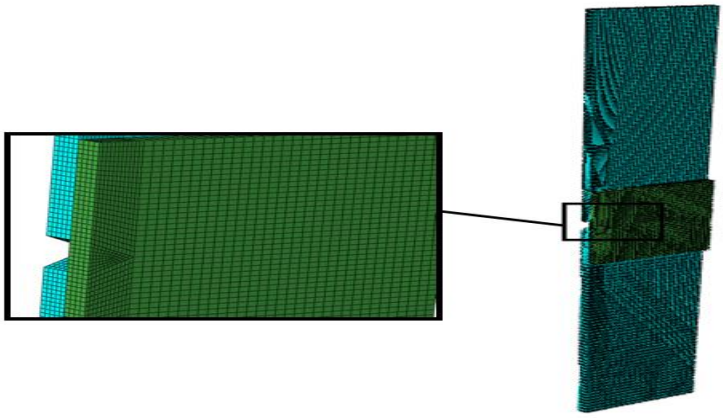

Fig. 2 Finite element mesh for the notched aluminum substrate and cohesively bonded CFRP patch

of the disbond.

One challenge is to experimentally measure the disbonding behavior of patch repaired metal substrates under load. In this regard, acoustic emission a nondestructive technique, offers a means for monitoring and detection of disbond damage events due to the application of stress. Acoustic emission is widely used for the quality control of structures (Grosse 2008, NDT, AMSY 2009), the monitoring of engineering structures (bridges and buildings) and also for petrochemical pressure vessels.

Chukwujekwu *et al*. (2007) has shown that the acoustic emission technique can be used to detect the disbond of the bonded assemblies. Defects, or events of random damage (ERD) that occur during disbonding are detectable by capturing their emitted acoustic waves using piezo-electric sensors that transform propagating stress waves to an analog electrical signal which are then digitized and subsequently analyzed. As stress is applied, the sensors detect the onset and evolution of defects, and evaluate the disbonding phenomena. Prior studies have shown that amplitudes corresponding to disbonding events are of weak intensity compared to those detected during the metallic substrate defect acoustic signals (Gu 2012, Ohtsu 2015). Damage events can then be separated localized and characterized in terms of disbanding.

In the majority of the aforementioned studies, patch disbonding was analyzed as a pre-existing imperfection and not calculated. The objective of this study was to investigate the location and the characterization of the disbond between a notched aluminum plate with a CFRP patch. The numerical analysis is done using the finite element method the results of which are validated by detecting the disbond experimentally using the acoustic emission technique.

2. Materials and methods

2.1 Numerical modeling

The numerical modeling of the disbonding phenomenon is carried out using Abaqus Finite Element (FE) software (Abaqus Analysis User's Guide 6.13). The simulation is based on the following four sections:

2.1.1 Geometrical model

Fig. 1 represents the geometry of the bonded joint with dimensions taken from ASTM647 standards.

Fig. 2 shows the finite element mesh of the numerical model, where only the patch and the substrate are required to be meshed since the adhesive thickness is negligible compared to the CFRP patch and aluminum substrate. The adhesive is modeled as an cohesive interface between the

Table 1 Contact properties used to define cohesion in the finite element model between the patch and the substrate

Elastic properties			Damage Properties			
			Yield stress			Damage Evolution
Normal Strength [MPa/mm]	Shear 1 Strength [MPa/mm]	Shear 1 Strength [MPa/mm]	Normal [MPa]	Shear 1 [MPa]	Shear 2 [MPa]	Fracture energy density [mJ/mm^2]
25200	10800	10800	10	15	15	0.3

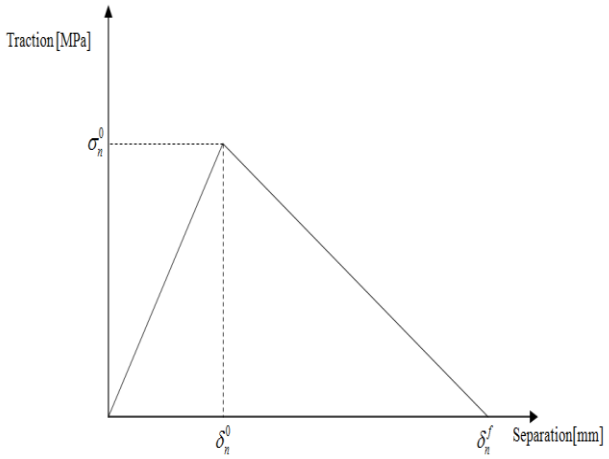

Fig. 3 Typical traction-separation response of the contact

patch and the aluminum surface. The finite element mesh was generated to have the same subdivisions so that both parts match at contact in order to get the best approximation of the disbonding, with node to node contact established at the interface.

2.1.2 Cohesive contact modeling

The contact between the patch and the substrate is considered to have a cohesive behavior with the properties shown in Table 1. The opening displacement [mm] of the cohesive interface in the normal direction and both shear directions is related to the applied stress [MPa] and the interface strength. We have used the same method used by Young and al. (1989) in study on the behavior of the adhesive layer of a bonded joint.

Fig. 3 shows the contact cohesive behavior between the two surfaces in one direction; in reality it is a combination of the three directions (normal σ_n, shear 1 σ_s and shear 2 σ_i). The contact stiffness increases linearly to reach the yield stress σ_n^0 (equivalent to yield displacement δ_n^0) as shown in Fig. 3 and then the stiffness is considered to decrease linearly until the failure displacement δ_n^f. Beyond this value the contact is fully opened. The surface-base cohesive behavior is a feature included in Abaqus which allows for the modeling of a generalized traction-separation behavior between surfaces. The surface-base cohesive behavior (Benzeggagh *et al*. 1996, Camanho *et al*. 2002) is intended for simulation in situations where interface thickness is negligible. The build-in traction-separation model assumes initially linear elastic behavior followed by initiation and evolution of damage, as shown in Fig. 3.

Table 2 Mechanical properties of the materials used in this study

Mechanical properties	Materials		
	AL 7075-T6	Carbone/ Epoxy	Adhesive (Araldite)
Longitudinal Young's Modulus (Mpa)	71700	130000	2520
Transversal Young's Modulus (Mpa)	71700	9000	1008
Longotudinal Poisson Ratio	0.33	0.33	0.36
Transversal Poisson Ratio	0.33	0.53	0.36
Hardness, HV	39.1	-	-
Elongation at Break (%)	10	-	-
Shear Modulus (Gpa)	28000	-	0.954
Yield Strength (Mpa)	503	-	-

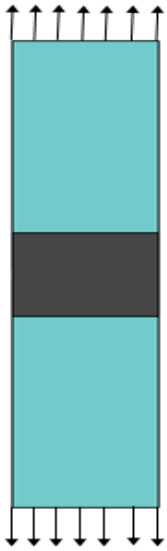

Fig. 4 Applied boundary conditions simulating uniaxial tension

2.1.3 Materials properties

The properties of the different components of the bonded joint are showed in Table 2 (Sohail 2014).

2.1.4 Loading conditions

The finite element model boundary conditions are shown in Fig. 4. A load of 70 MPa is applied on the edges of the plate to create uniaxial tensile loading.

2.2 Experimental

Tension tests were carried out on prenotched samples with and without a CFRP patch, as illustrated in Fig. 1.

2.2.1 Sample preparation

The materials used in this study were 7075-T6 aluminum, carbon fiber reinforced composite and "Araldite" a two-part epoxy adhesive. The 7075-T6 specimens were obtained as standard flat stock with composition shown in Table 3. The 7075-T6 material is a

Table 3 Composition of Aluminum 7075-T6 (Alcoa Inc)

Wt.%	Cr	Cu	Fe	Mg	Mn	Si	Ti	Zn	Other	Al
Min.	0.18	1.2	-	2.1	-	0.4	-	5.1	-	-
Max.	0.28	2.0	0.5	2.9	0.3	0.8	0.2	6.1	0.5	Bal

Table 4 Mechanical properties of test materials

Mechanical properties	Materials		
	AL 7075-T6	CFRP	(Araldite)
Young's Modulus Longitudinal (Mpa)	71700	130000	2520
Transverse Young's Modulus (Mpa)	71700	9000	2520
Longitudinal Poissons Ratio	0.33	0.33	0.36
Transverse Poissons Ratio	0.33	0.53	0.36
Hardness, HV	39.1	-	-
Elongation at Break (%)	10	-	-
Shear Modulus (Mpa)	28000	-	0.954
Yield Strength (Mpa)	503	-	-

solution heat-treated and precipitation-hardened alloy that was manufactured from rolled sheet and the roll direction of the material was aligned with the tensile axis.

The CFRP plate where prepared by Sohail *et al*. (2015) which consisted of a mix of woven fibers internally and aligned fibers on the outermost layers. Repair patches were cut from the plate and fibers were aligned with the tensile test direction. The Araldite epoxy adhesive from Huntsman.

Advanced Materials was prepared according to manufacturer instructions and selected as representative of those used commercially in the aerospace industry. The bond strength of the epoxy adhesive to aluminum was reported to be 2 MPa by the manufacturer. The mechanical properties for the materials are listed in Table 4 and used as input to the finite element models.

The tension test specimens consisted of notched aluminum plates, with and without a repair patch. The samples were cut and notched with dimensions shown in Fig. 1. Preparation of patch repaired samples involved cleaning, to create a dry and grease-free surface before applying the adhesive. Aluminum samples were hand abraded with emery-cloth and degreased with Acetone. The application of the adhesive on the substrate was done using a dual cartridge manual dispenser with a spiral mixing tip designed for this purpose from the manufacturer. Assembly of patch repaired specimens followed this sequence: (1) at room temperature, apply mixed adhesive to aluminum surface, (2) place patch onto adhesive with fibers aligned with tensile loading direction and (3) clamp assembly with 2 Mpa pressure for 24 hrs. This resulted in an adhesive layer of ~0.1 mm thickness. Literature suggests that a good adhesive layer thickness be in the range 0.05 to 0.1 mm.

2.2.2 Acoustic Emission (AE) acquisition

All specimens were tested using an Instron model 1331 (Fig. 5) servo hydraulic test machine (1989), at a crosshead displacement rate of 1 mm/min as shown in Fig. 7.

All tensile specimens were single-notched (Fig. 1) at the

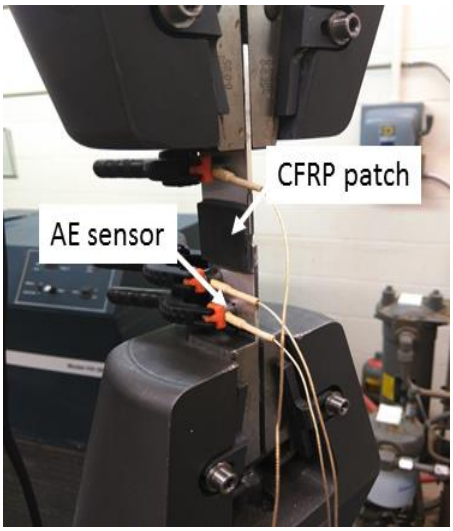

Fig. 5 Tensile test setup showing repair patch on aluminum specimen with three piezoelectric acoustic emission sensors clamped onto the aluminum specimen surface

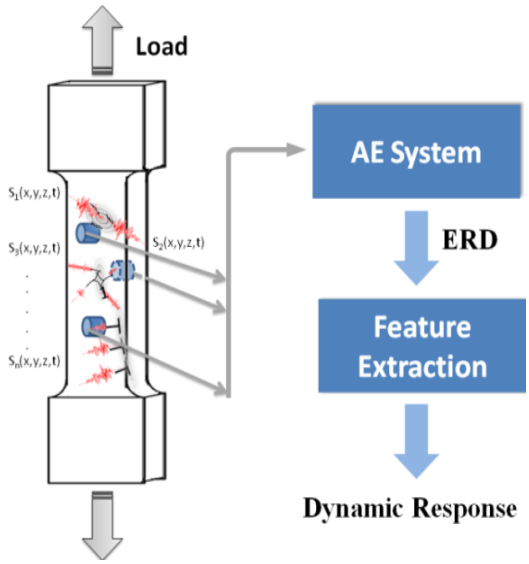

Fig. 6 Schematic view of the testing system: note example of three AE sensors that detect ERD and transmit signals to the AE System

mid-plane to localize the damage zone and concentrate damage events in the narrowed cross section. The simple tension test experiment with associated AE signals are shown schematically in Fig. 6 and Fig. 7, in which sensors are attached to the surfaces of the sample and allow for data flow. An example of an AE signal from a random event is illustrated in Fig. 7. Some useful definitions are: energy (the area beneath the waveform), amplitude (the maximum AE count within one waveform envelope, in dB), duration (the length of an AE waveform envelope in Nano second), and rise time (the time to reach the amplitude in Nano second).

The sensors are attached to the surface of the specimen (Fig. 6) to span the patched area and capture all detectable random damage events. Whether a damage event source is on the surface or embedded in the body generally does not affect the acquisition. The load data was synchronized with

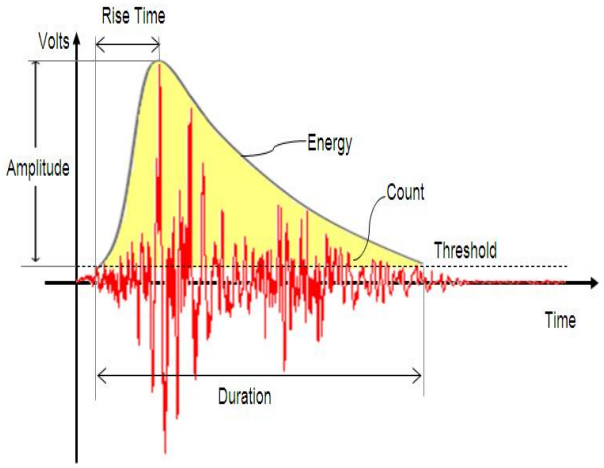

Fig. 7 Example of AE waveform from RE and associated terminology

the AE acquisitions. To acquire the AE signatures, three piezoelectric sensors (Physical Acoustics, Inc) were clamped to the surface of the specimen (with silicone grease in between) at positions to acquire signals in the region of the notches. The AE sensors have a resonant frequency and operating frequency range of ~250 kHz and 150-400 kHz, respectively. The resultant AE signatures were pre-amplified by a 40 dB pre-amplifier with a bandpass filter between 2.5 kHz and 3.8 MHz, before being fed to an AE system (AEP4, Vallen Systeme, Germany). The threshold for the data acquisition was selected to minimize the noise from the testing machine; this was done by installing the specimen in the testing machine with near zero loading and determining that there were no significant detectable signals at or below 32.5 dB, thus, this value was used as the threshold.

3. Results

The detection of disbonding between patch and plate was done using both numerical and experimental analysis. In section 3.1 we present the most significant results obtained from the numerical analysis and in 3.2 we present those obtained from the experimental analysis.

3.1 Numerical analysis results

Fig. 8 shows the Von Mises (VM) stress distribution resulting from tensile loading of a plain aluminum and patch repaired aluminum plate adhered face Fig 9 contains the stress in the patch. The highest stress concentration is located around the notch tip (Fig. 9), whereas the stress level in the patch of the plate is very low on the front side but the other side (which is stitched to the plate) is higher as shown in Fig. 9.

Fig. 9 shows the stress distribution for the patch. The stress distribution approximates the shape of the notch and is uniformly distributed along the notch axis beneath the patch (60 MPA). This region illustrates the redistribution of stress from the aluminum into the patch.

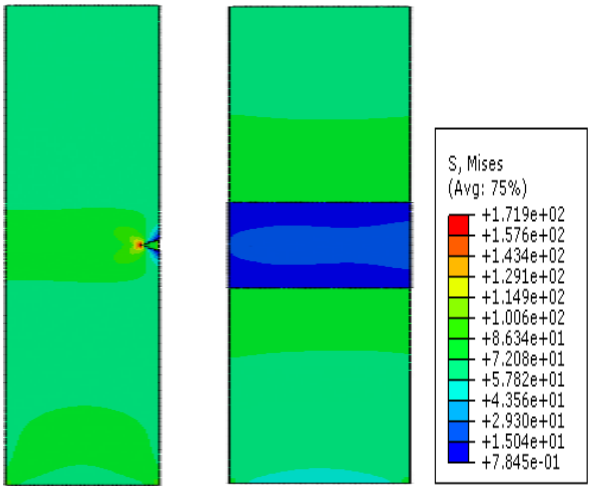

(a) (b)

Fig. 8 Von Mises stress (MPa) distributions from tensile loading of notched aluminum (a) plain aluminum plate and (b) repaired (but with patch removed to reveal stress in aluminum at interface)

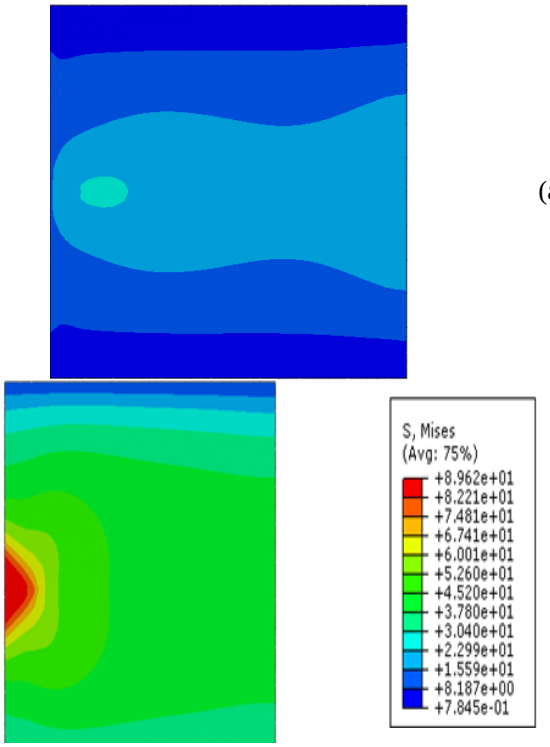

(a)

(b)

Fig. 9 Von Mises stress (MPa) distribution at (a) exterior patch surface and (b) patch/aluminum interface

Fig. 11 shows the contact status between the CFRP patch and aluminum plate. The disbond occurs close to the bond edge (upper and lower side) and along the notch axis of the bonded interface. The disbond area is greater than the bonded one. So we find that when repaired joints disbond there is also a reduction of the stress transfer into the patch.

Fig. 12 shows the disbonding areas for different fiber orientations (90°, 45°, 0°). The case of 90° fibers orientation means that the fibers are positioned parallel to

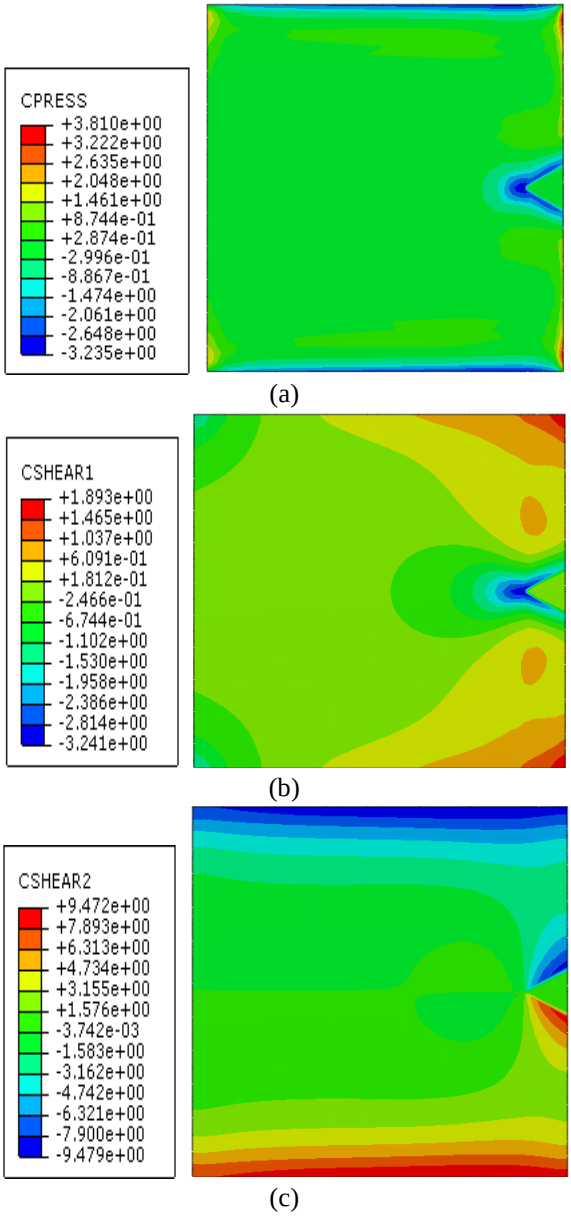

Fig. 10 Contact stresses (MPa) between the patch and the plate, (a) normal stress, (b) *x-y* shear stress and (c) *y-z* shear stress

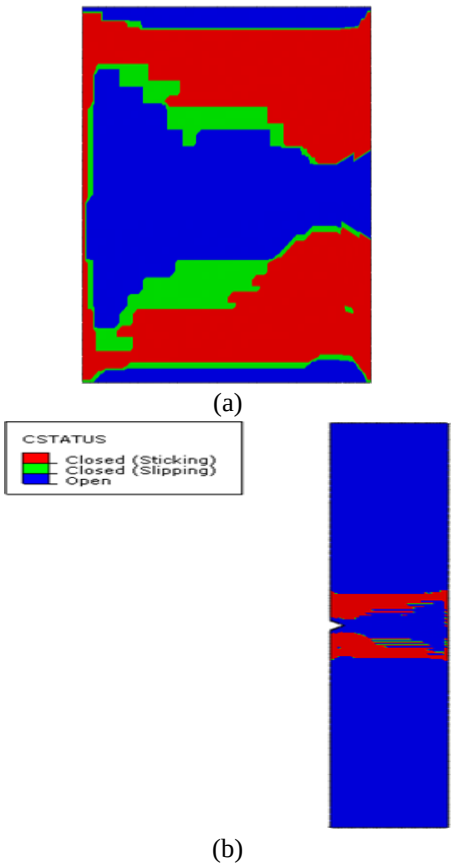

Fig. 11 Contact status between the patch and the plate(a) the patch, (b) the plate

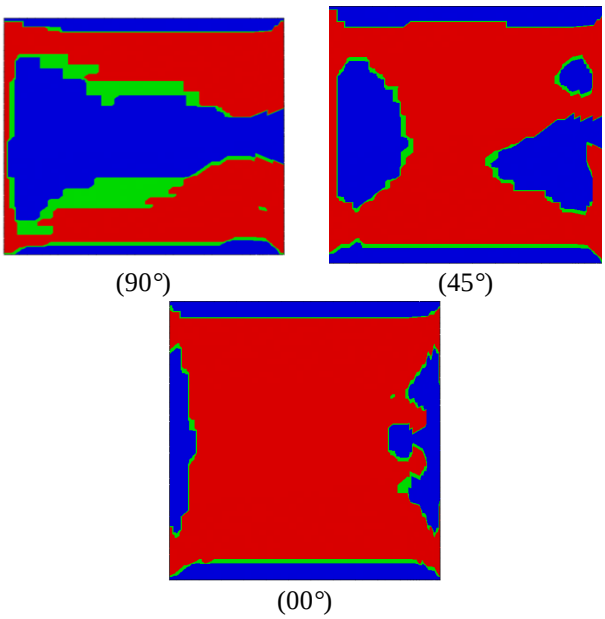

Fig. 12 Disbonding area (blue) between the patch and the plate for different patch fiber orientations

the tensile axis and 0° means that the fibers are aligned perpendicularly to the tensile axis. Comparing the different fiber orientation reveals a strong decrease on disbonding area when the fiber orientation changes from a parallel to a perpendicular position. This leads to many possible stress distributions based on crack geometry, fiber orientation and patch adhesive properties.

Fig. 13 shows the effect of the doubling the adhesive strength on the disbonding area between the patch and its substrate. This Figure shows that there is a reduction in the disbonded area when the adhesive strength is doubled. A controlling factor here is the normal stress component which leads to failure at the interface and arises from bending forces.

3.2 Experimental results

In ordered to validate the numerical analysis, an experimental study was carried out to measure the disbonding between the patch and the aluminum substrate using the acoustic emission technique. Fig. 14 (a) and (b) shows the load and AE event amplitude versus time curves

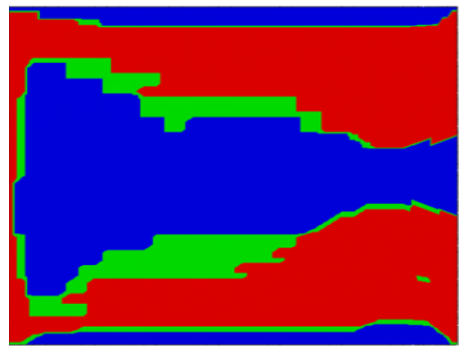

(a)

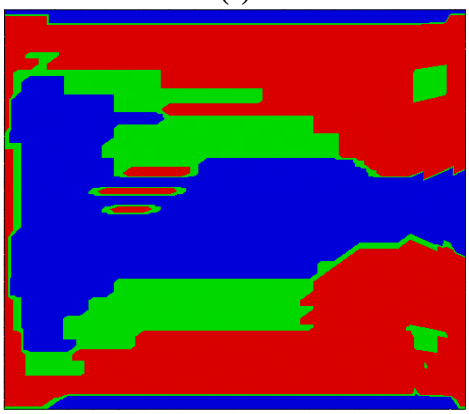

(b)

Fig. 13 Comparison of disbonding area of the patch, (a) as Fig. 13(a) and (b) doubled adhesive strength

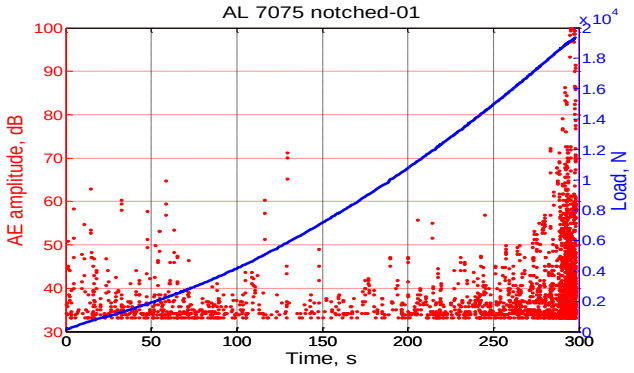

(a)

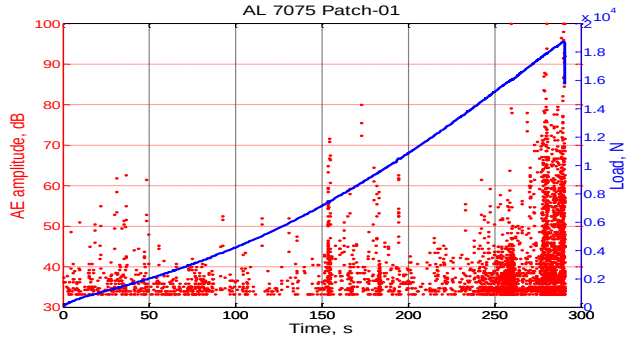

(b)

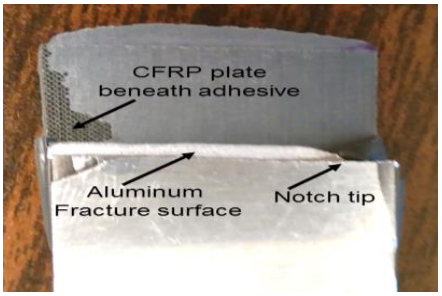

(c)

Fig. 14 Tensile test of (a) plain aluminum with notch and (b) patch repaired notched aluminum plate showing load and acoustic emission event amplitudes; (c) light micrograph of fractured patched repaired sample showing the disbonded interface

of both notched and patch repaired notched specimens. The load vs time curves are very similar for both repaired and unrepaired specimen. Each curve contains three distinct regions with linear elastic response up to 70 sec of time, then nonlinear response up to 200 sec followed by a linear response until final fracture occurs. When comparing the plain sample to the patched, the load response does not reflect any strengthening influence into the aluminum sample. Also shown in Fig. 14 (a) and (b) are the amplitude of acoustic events that were collected during the tests. Fig. 7 shows that the amplitude is the peak value of the acoustic waveform which is directly related to the magnitude of the damage event. We see in Fig. 14(a) that acoustic events occur during each of the three distinct regions described above, which means they begin during the early loading stages of elastic deformation and continue until failure. We also observe that a large quantity of events are present and have a varying distribution during the course of the test. The largest amplitude events occur near final failure, no doubt a consequence of macro fracture of the aluminum. Other groups are associated with the initiation and propagation of the crack from the starting notch. Of interest is the comparison to Fig. 14(b) during the 150-200 and 250-300 sec. periods of the test, since this region has a strong burst of events reaching ~70dB. We associate this burst with the disbonding of the patch at the adhesive/aluminum interface. This interfacial disbonding was confirmed experimentally and is shown in Fig. 14(c). Gu *et al*. found that adhesive disbonding occurs when the patch is thick (2 mm) and that a combined disbond and patch failure occurs when the patch is thin (0.125 mm) which confirm our results.

In order to better resolve the disbond behavior, we show Fig. 15 (a) and (b) that compare the number of acoustic events that occurred during the tests. Fig. 15(a) shows a relatively constant occurrence of damage events until ~350 sec, with a spike in events due to final fracture of the sample. In comparison, Fig. 15(b) reveals damage event bursts between 130-300 sec. Such bursts are attributed to the patch disbonding as strain in the aluminum sample increased with time. We expect that as strain is increased, the emanating crack from the starting notch in the aluminum would be suppressed by the patch. However, since the bonding strength of the adhesive to the aluminum was relatively low, the adhesive/aluminum interface disbonded early in the loading cycle and little crack suppression was realized. Our finite element analyses (see

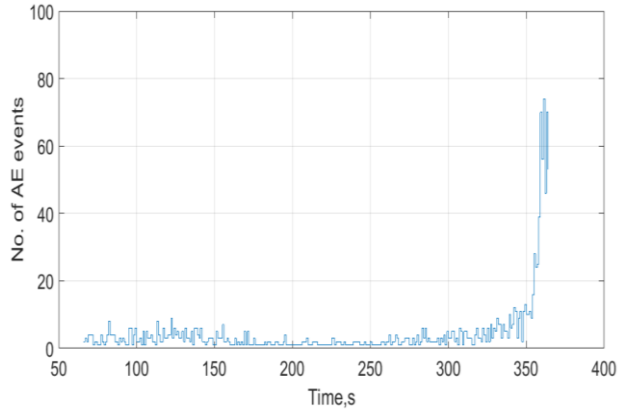

(a)

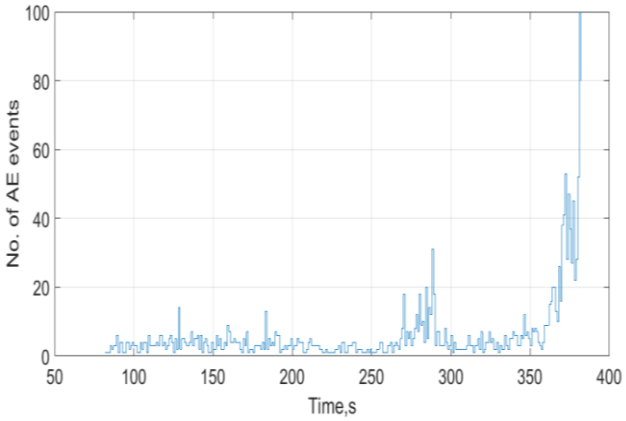

(b)

Fig. 15 the AE events for unrepaired (a) and repaired (b) sample

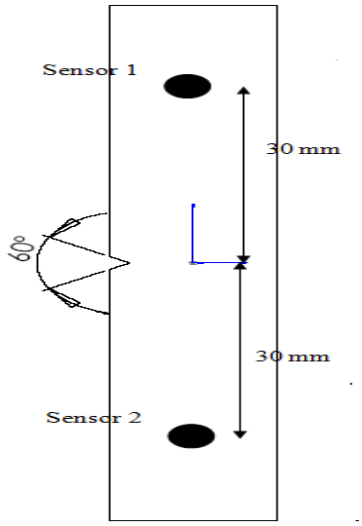

Fig. 16 Sensors positions

Fig. 13) shows that as the adhesive/aluminum bond strength increased, the ability of the patch to suppress crack propagation proportionately increased. The experimental results presented in Figs. 14 and 15 serve as confirmation of the interfacial contact obtained with our finite element model shown in Fig. 11.

The source of acoustic emission location is needed to realize which part of the sample is damaged and/or disbonded. For this purpose a specific acoustic emission setup was done on the patch repaired aluminum sample to detect the disbonding location at the interface.

Fig. 16 shows the positioning of sensors, selected to identify the damage/disbonding locations. Two sensors are setup along the *Y*-direction. Since the specimen is a narrow 1-D localization of disbonding was achieved with acceptable spatial resolution, allowing us to plot source event location in the *Y*-direction only (tensile axis).

Fig. 17 shows results of damage event source location and the time of occurrence during the tension test of (a) unrepaired and (b) repaired aluminum plates. This plot is very useful as it reveals when and where the damage events occur. We see that in the early stages of testing the patch does protect the notch from the stress amplification. This is evident when comparing to the unrepaired sample where we can notice some events at the beginning of the test, which are not evident in the patched plate. The difference between both samples occurs in the middle stage of testing. For the repaired samples, we noticed a cluster of emission sources over the entire patch length and for the unrepaired plate, the source location are only located in the notch axis. This cluster is thought to be the result of stretching the adhesive under tension. As load increases, the amount of detected sources decreases which means that the patch has reached

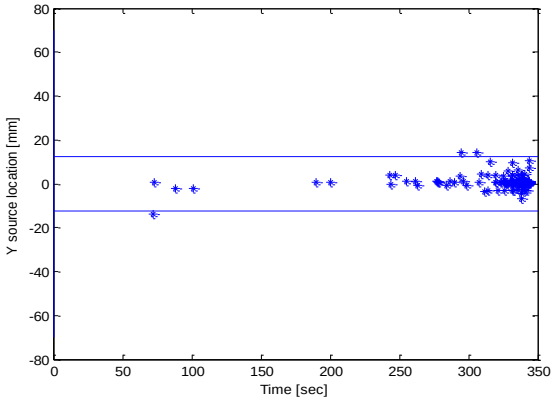

(a)

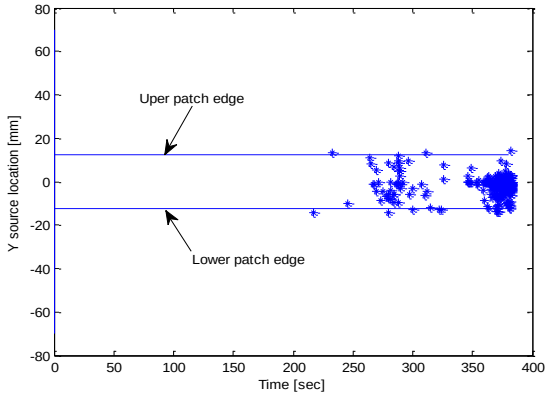

(b)

Fig. 17 AE source location in Y direction and the emission time of (a) unrepairedand (b) patch repaired aluminum plates

its failure limit Beyond that, there's still evidence for adhesive stretching however the detected sources are far from the crack. The cluster of damage events is located on one side of the crack which means that the adhesive fails on one side and remains adhered on the other side as shown in Fig. 17. Chukwujekwu and al. found a disbond around a crack in a repaired plate, this confirms that the disbonding occurs around defects as found by our study.

4. Conclusions

This study has allowed us to investigate the location and the characterization of the disbond between a notched aluminum plate with a CFRP patch. We found that the adhesive strength and fiber orientation of the patch were key parameters that determine patch repair effectiveness. We also found that with a low adhesive strength, the patch serves as a stress shield by protecting the notch only in the earliest stages of tensile loading. Our AE analysis revealed that the adhesive is the first part of the joint to disbonding. Further numerical analyses revealed damage locations beneath the patch where disbonding regions were located around the notch and close to the patch free edges. The AE data analysis confirmed the prediction of disbonding obtained by the finite element model.

Acknowledgements

Thanks to Prof. Gang. Qi, for welcoming in the Medical Acoustic Laboratory, University of Memphis, Memphis, TN, USA.

References

Abaqus Analysis User's Guide (6.13).

AEP4, Vallen Systeme, Germany.

Albedah, A., Khan, S.M., Benyahia, F. and Bouiadjra, B.B. (2015), "Experimental analysis of the fatigue life of repaired cracked plate in aluminum alloy 7075 with bonded composite patch", *Eng. Fract. Mech.*, **145**, 210-220.

Albedah, A., Khan, S.M., Benyahia, F. and Bouiadjra, B.B. (2016), "Effect of load amplitude change on the fatigue life of cracked Al plate repaired with composite patch", *Int. J. Fatigue*, **88**, 1-9.

Alcoa Inc. http://www.alcoa.com

ASTM E647-15, Standard Test Method for Measurement of Fatigue Crack Growth Rates. Active Standard ASTM E647 | Developed by Subcommittee: E08.06, Book of Standards Volume: 03.01.

Baker, A. (1993), "Recent advances in bonded composite repair technology for metallic aircraft components", Metals and Materials Society, Warrendale, PA.

Baker, A. (1995), "Bonded composite repair of metallic aircraft components-Overview of disbonding activities", AGARD, CP-550.

Baker, A. (1997), "On the certification of bonded composite repairs to primary aircraft structures", *Proceeding of the 11th Int Conference on Composite Materials*, Vol. 1, 1-24.

Baker, A., Rose, F. and Jones, R. (2003), *Advanced in the Bonded Composite Repair of Metallic Aircraft Structures*, Volume I and II, Elsevier.

Benchiha, A. and Madani, K. (2015), "Influence of the presence of defects on the stresses shear distribution in the adhesive layer for the single-lap bonded joint", *Struct. Eng. Mech.*, **53**(5), 1017-1030.

Benchiha, A., Madani, K., Touzain, S., Feaugas, X. and Ratwani, M. (2016), "Numerical analysis of the Influence of the presence of disbond region in adhesive layer on the stress intensity factors (SIF) and crack opening displacement (COD) in plates repaired with a composite patch", *Steel Compos. Struct.*, **20**(4), 951-962.

Benzeggagh, M.L. and Kenane, M. (1996), "Measurement of mixed-mode delamination fracture toughness of unidirectional glass/epoxy composites with mixed-mode bending apparatus", *Compos. Sci. Technol.*, **56**, 439-449.

Bouiadjra, B.B., Benyahia, F., Albedah, A., Bouiadjra, B.A.B. and Khan, S.M. (2015), "Comparison between composite and metallic patches for repairing aircraft structures of aluminum alloy 7075 T6", *Int. J. Fatigue*, **80**, 128-135

Bouiadjra, B.B., Ouinas, D., Serier, B. and Benderdouche, N. (2008), "Disbond effects on bonded boron/epoxy composite repair to aluminum plates", *Comput. Mater. Sci*., **42**(2), 220-227.

Camanho, P.P. and Davila, C.G. (2002), "Mixed-mode decohesion finite elements for the simulation of delamination in composite materials", NASA/TM-2002-211737, 1-37.

Denney, J.J. (1997), "Characterization of disbonding effects on fatigue crack growth behavior in aluminum plate with bonded composite patch", *Eng. Fract. Mech.*, **57**(5), 507-525.

Elhannani, M., Madani, K., Mokhtari, M., Touzain, S., Feaugas, X. and Cohendoz, S. (2016), "A new analytical approach for optimization design of adhesively bonded single-lap joint", *Struct. Eng. Mech.*, **59**(2), 313-326.

Fujimoto, S.E. and Sekine, H. (2007), "Identification of crack and disbonding fronts in repaired aircraft structural panels with bonded FRP composite patches", *Compos. Struct.*, **77**(4), 533-545.

Grosse, C.U. and Ohtsu, M. (2008), *Acoustic Emission Testing*, Springer-Verlag Berlin Heidelberg.

Gu, J.U., Yoon, H.S. and Choi, N.S. (2012), "Acoustic emission characterization of a notched aluminum plate repaired with a fiber composite patch", *Compos. Part A: Appl. Sci. Manuf.*, **43**(12), 2211-2220.

Huntsman Advanced Materials company. www.araldite2000plus.com

Instron: http://www.instron.fr.

Khan, S.M., Benyahia, F., Bouiadjra, B.B. and Albedah, A. (2014), "Analysis and repair of crack growth emanating from v-notch under stepped variable fatigue loading", *Procedia Eng.*, **74**, 151-156.

Mohamed, B. and Bouiadjra, B.B. (2016), "Analysis of the adhesive damage for different patch shapes in bonded composite repair of corroded aluminum plate", *Struct. Eng. Mech.*, **59**(1), 123-132.

Mohammed, S.M.A.K. (2015), "Bonded composite patch repair of aluminium plates under fatigue loading", PhD Tthesis, King Saudi University, Saudi Arabia. Riyadh.

Nano 30, Physical Acoustics, Inc., Princeton, NJ, USA.

Non Destructive Testing (NDT) center, https://www.nde-ed.org

Ohtsu, M. (2015), *Acoustic Emission and Related Non-destructive Evaluation Techniques in the Fracture Mechanics of Concrete: Fundamentals and Applications*, Woodhead Publishing.

Okafor, A.C., Singh, N. and Singh, N. (2007), "Acoustic emission detection and prediction of fatigue crack propagation in composite patch repaires using neural networks", *AIP Conference Proceedings*, Vol. 894, No. 1, 1532-1539.

Ouinas, D., Bachir Bouiadjra, B., Himouri, S. and Benderdouche, N. (2012), "Progressive edge cracked aluminium plate repaired

with adhesively bonded composite patch under full width disband", *Compos. Part B: Eng.*, **43**(2), 805-811.
SOL Inc. (2013), http://www.comsol.com
Vallen system GmbH (2009), Acoustic emission systeme AMSY - 5 system description, Vallen Systeme GmbH.
Wegman, R.F. (1989), *Surface Preparation Techniques for Adhesive Bonding*, Reprint Edition, Text Book.
Young, A., Rooke, D.P. and Cartwright, D.J. (1989), "Numerical study of balanced patch repairs to cracked sheets", *Aeronaut. J.*, **93**, 327-334.

CC